



A thiol-ene microfluidic device enabling continuous enzymatic digestion and electrophoretic separation as front-end to mass spectrometric peptide analysis

Lu, Nan; Sticker, Drago; Kretschmann, Andreas; Petersen, Nickolaj J; Kutter, Jörg P

Published in:
Analytical and Bioanalytical Chemistry

DOI:
[10.1007/s00216-020-02609-5](https://doi.org/10.1007/s00216-020-02609-5)

Publication date:
2020

Document version
Publisher's PDF, also known as Version of record

Citation for published version (APA):
Lu, N., Sticker, D., Kretschmann, A., Petersen, N. J., & Kutter, J. P. (2020). A thiol-ene microfluidic device enabling continuous enzymatic digestion and electrophoretic separation as front-end to mass spectrometric peptide analysis. *Analytical and Bioanalytical Chemistry*, 412(15), 3559-3571. <https://doi.org/10.1007/s00216-020-02609-5>



A thiol-ene microfluidic device enabling continuous enzymatic digestion and electrophoretic separation as front-end to mass spectrometric peptide analysis

Nan Lu¹ · Drago Sticker² · Andreas Kretschmann¹ · Nickolaj J. Petersen¹ · Jörg P. Kutter¹

Received: 18 February 2020 / Revised: 13 March 2020 / Accepted: 18 March 2020 / Published online: 6 April 2020
© Springer-Verlag GmbH Germany, part of Springer Nature 2020

Abstract

One of the most attractive aspects of microfluidic chips is their capability of integrating several functional units into one single platform. In particular, enzymatic digestion and chemical separation are important steps in processing samples for many biochemical assays. This study presents the development and application of a free-flow electrophoresis microfluidic chip, and its upstream combination with an enzyme microreactor with immobilized pepsin in the same miniaturized platform. The whole microfluidic chip was fabricated by making use of thiol-ene click chemistry. As a proof of concept, different fluorescent dyes and labeled amino acids were continuously separated in the 2D electrophoretic channel. The protease pepsin was immobilized using a covalent linkage with ascorbic acid onto a high-surface monolithic support, also made of thiol-ene. To show the potential of the microfluidic chip for continuous sample preparation and analysis, an oligopeptide was enzymatically digested, and the resulting fragments were separated and collected in a single step (prior to mass spectrometric detection), without the need of further time-consuming liquid handling steps.

Keywords Free-flow electrophoresis · Microfluidics · Thiol-ene polymers · Continuous sample preparation · Immobilized enzyme reactors · Online digestion

Introduction

Enzymatic cleavage is a commonly used sample preparation step, e.g., during the production and evaluation of biopharmaceutical drug candidates [1, 2]. The proteolytic digestion is traditionally performed in bulk by mixing enzyme and substrate in solution and incubating overnight [3] in order to obtain sufficient amounts of digested product for further biopharmaceutical analysis. The proteolysis procedure remains a limiting step in many analytical workflows, often suffering from enzyme degradation by autolysis and long reaction times [4,

5]. The approach where enzymes are immobilized on solid supports has become an intriguing alternative, due to its inherent advantageous features, such as considerably reduced digestion times, increased stability of the enzymes, and protection from undesirable auto-digestion [6, 7]. Particularly, the most powerful benefit of immobilized enzyme reactors (IMERs) is the convenient reusability of the effective biocatalyst [8], without any extra and costly procedure to recycle and purify, since in some cases very rare and hence expensive enzymes are needed in the laboratory and during biotechnological production. IMERs are commonly operated in a pump-controlled continuous-flow manner [9, 10], thus making it an attractive strategy to combine IMERs online with (continuous) separation workflows.

IMERs can be miniaturized and incorporated into microfluidic chip-based devices, thus further reducing consumption of enzymes, offering highly efficient immobilization, overall lower costs for reagents, and portability [11, 12]. Moreover, microchip-based reactors provide more benefits when compared with microcapillary reactors, such as easily and directly controlled flow rates [13]. Most importantly, microfluidics offers the unique possibility to integrate enzyme

Electronic supplementary material The online version of this article (<https://doi.org/10.1007/s00216-020-02609-5>) contains supplementary material, which is available to authorized users.

✉ Jörg P. Kutter
jorg.kutter@sund.ku.dk

¹ Department of Pharmacy, University of Copenhagen, Universitetsparken 2, 2100 Copenhagen, Denmark

² Global Research Technologies, Novo Nordisk AS, 2760 Måløv, Denmark

reactors with subsequent analytical functionalities in the same unit, such as separation and detection.

Microfluidic devices have commonly been manufactured with conventional wet etching and lithography techniques, using hard materials like glass [14] and silicon [15]. However, this approach calls for labor-intensive and time-consuming processes [16]. Soft lithography techniques used for polymer-based materials are often preferred, because they do not rely on costly and laborious fabrication procedures. Thiol-ene-based polymeric materials as alternatives to the widely used poly(dimethyl)siloxane (PDMS) have gained increased interest because of their favorable polymerization characteristics and especially a very economic fabrication procedure [17]. The specific photopolymerization reaction involves the addition of a thiol functionality to an alkene functionality to form a thioether [18, 19], under exceptionally fast UV curing conditions [20, 21]. The cross-linked polymers exhibit flexibility, strong mechanical strength, low contraction stress eliminating warpage, and homogeneous networks [22]. The greatest advantage of thiol-ene polymers is their potential to provide easy access to surface functionalization, by making use of different stoichiometric ratios of the two monomers during polymerization to produce excess sulfhydryl or allyl functional groups, respectively, on the surfaces of the channels [23, 24]. To prepare efficient enzyme reactors, a large surface area is typically needed. To provide sufficiently large surface areas in microchannels, porous monoliths can be introduced. This is elegantly done using emulsions of thiol-ene materials dispersed in an immiscible liquid serving as the continuous phase [25, 26]. After polymerization, the resulting monolithic bed is composed of fully connected beads providing a large surface area as well as a strong connection to the rest of the substrate to keep the monolithic bed inside the channel. In this study, enzymes were immobilized on such monolithic supports through covalent linkage of ascorbic acid [26]. This approach offers a simple and rapid way to anchor enzymes to microchannels by coupling free amine groups on the surface of the monolith and the primary amino groups of enzymes. IMERs fabricated in this way are very suitable to be integrated with separation units within microfluidic devices.

Recently, efforts have been made to develop a combined miniaturized, polymer-based platform for proteolytic digestion and separation. Capillary electrophoresis has been shown to be a very powerful tool for the separation of enzymatic reaction products, because of its high efficiency and fairly straightforward coupling with IMERs in both online and offline modes [10, 27, 28]. In CE-integrated IMER devices, enzymes are bound to the inner capillary surface to carry out the catalytic reaction; subsequently, the separation and detection of any resulting products are accomplished online at the downstream end of the same capillary. Enzymatic microreactors have been accomplished through open-tubular [28–31], packed-type [8, 32–34], and monolithic techniques

[35–40] based on capillaries. The online coupling of microchips with IMERs is rather straightforward since microfluidic chips are commonly operated under laminar flow conditions. Sakai-Kato et al. fabricated an online microreactor by preparing an in situ trypsin-encapsulated sol-gel onto a poly(methyl methacrylate) (PMMA) microchip, integrated with electrophoretic separation in the same device [41].

Free-flow electrophoresis (FFE) is a viable alternative to on-chip CE. Moreover, FFE is a useful tool for preparative separation, since the direction of separation is different from that of the bulk flow [42]. Micro free-flow electrophoresis (FFE) is a continuous separation technique, where electrophoresis is performed on a sample stream as it flows through a carrier medium in a planar chamber [43, 44]. More specifically, sample flow is exposed to the electric field that is applied perpendicularly and the trajectories of the components are deflected spatially according to their mobilities. This technique has a high potential to be used for preparative purposes.

Miniaturization of FFE (μ FFE) is an attractive approach in both the preparative and analytical fields due to the fast separation, portability, high surface-to-volume ratio that can improve heat dissipation, and small sample volumes [45]. Thus, μ FFE offers a lot of potential to be combined with other fluidic units towards full lab-on-a-chip systems [46, 47], among those various chemical reaction and sample pretreatment techniques [48–50]. So far, μ FFE has not been integrated with an enzyme microreactor yet. Sample transfer and other handling steps could be eliminated by combining reactor and continuous flow separator seamlessly, thus allowing the combined platform to be more automatable. Digestion products or metabolites can then be collected and used for downstream applications after the micropreparative process.

In this paper, we report an all-thiol-ene microfluidic-based device fabricated using a double-molding technique, comprising an enzymatic reactor in-line with a continuous separation FFE. Firstly, the device was successfully tested for free-flow electrophoretic separation of fluorescent dyes, amino acids, and peptides. Separation efficiencies on the μ FFE chip were characterized under different conditions, such as electric field strengths and buffer flow rates. Then, pepsin was immobilized on the thiol-ene monolithic support through an ascorbic acid linker, and integrated with the FFE unit. Real-time fluorescence detection was used for monitoring the separation process of intrinsically fluorescent compounds or labeled analytes. For peptides, which are not natively fluorescent, offline mass spectrometry detection was applied after collection from the outlets of the device. The hyphenation of IMER and μ FFE enables flexible and robust analysis in an online manner and circumvents manual steps when transferring digestion products from the microreactor to the electrophoretic separation.

Materials and methods

Chemicals and reagents

Pentaerythritol-tetrakis(3-mercapto propionate) (“tetrathiol”), triallyl-1,3,5-triazine-2,4,6(1H,3H,5H)-trione (“triallyl”), 4-(2-hydroxyethyl)piperazine-1-ethane sulfonic acid (HEPES), 2-(cyclohexylamino)ethanesulfonic acid (CHES), 2',7'-dichlorofluorescein, rhodamine B, rhodamine 6G, fluorescein isothiocyanate isomer I (FITC), sec-butylamine, L-aspartic acid, [Glu¹]-fibrinopeptide B human (Glu-fib), 2-(boc amino)ethanethiol, L-ascorbic acid (ASA), and pepsin from porcine gastric mucosa (lyophilized powder ≥ 2500 U/mg) were all obtained from Sigma-Aldrich (Brøndby, Denmark). Glycine, sodium hydroxide, and hydrochloric acid were purchased from Merck (Darmstadt, Germany). The Sylgard 184–poly(dimethylsiloxane) (PDMS) elastomer kit and (hydroxypropyl)-methylcellulose (HPMC) were bought from Dow Corning (Midland, MI, USA). Immobilized pepsin beads were purchased from Thermo Fischer Scientific (Waltham, MA, USA). Lucirin TPO-L was obtained from BASF (Ludwigshafen, Germany).

Stock solutions of 2',7'-dichlorofluorescein, rhodamine B, and rhodamine 6G were prepared in methanol at a concentration of 4 mg ml^{-1} . Mixture sample solutions were diluted with methanol/water (1:1, v/v) at final concentrations of $20 \text{ } \mu\text{g ml}^{-1}$. FITC-amine derivatives were prepared as follows: sec-butylamine, glycine, and aspartic acid were dissolved in 20 mM borate at pH 9 with final concentrations of 10 mM each. A total of 4 mg of FITC was dissolved in 50 μl DMSO and diluted to 1 mg ml^{-1} with 20 mM borate at pH 9. Derivatization of individual amines was performed by mixing 100 μl FITC solution and 400 μl amine, and the reaction was kept in the dark overnight. Final sample solutions were prepared by mixing stock solutions of FITC-amines and then diluting with running buffer. All the solutions were degassed and filtered right before the experiments to minimize bubbles and other interferences.

Fabrication of the microfluidic chip

A double-molding technique was used to fabricate the thiol-ene microfluidic microchips described elsewhere in detail [23]. Computer-aided design software (Autodesk Inventor Professional, 2015) was used to draw the chip structures. The master mold on a PMMA plate was obtained by high-precision milling (Minitech 3, Minitech Machinery Corp., Norcross, GA, USA). The dimensions of the channels were measured using a Dektak[®]XT stylus profiler (Bruker, Billerica, MA, USA). The second mold was made by pouring PDMS into the PMMA mold and curing for 2 h at 80 °C. A stoichiometric mixture of thiol and ene monomers was then poured into the PDMS replica mold and exposed to UV light

for 9 s on each side (160 mW cm^{-2} at 365 nm, Dymax EC 5000 Series UV curing flood lamp, Dymax Corp, Torrington, CT, USA). The two thiol-ene slabs were removed from the PDMS molds and aligned to each other manually, then cured under UV lamp for an additional 5 min to finalize the bonding process.

Monolith fabrication

The in situ polymerized thiol-ene monolith was prepared based on our previous work [26]. We prepared a mixture of 60% excess ene thiol-ene in methanol (80% w/w), while methanol was also used as the porogen. The emulsion was magnetically stirred in a sealed well plate at 1500 rpm for 5 min. 0.2% (v/v) photoinitiator (10% Lucirin TPO-L in ethanol) was added while stirring and mixed for another 5 min protected from light. All the inlets and outlets of the chips were sealed closed with tape other than the two used to access the microreactor. The emulsion was injected into the middle inlet (Electronic Supplementary Material (ESM) Fig. S1d) to fill the channel using a pipette, and photopolymerization was performed immediately using collimated light from a UV lamp (15 s, 20.5 mW cm^{-2} at 365 nm, LS-100-3C2 near UV light source, Bachur & Associates, Santa Clara, CA, USA). In this work, a 3D-printed photomask was used to define the portion of the microfluidic channel where the monolith was polymerized. As shown in ESM Fig. S1c and d, the opening in the mask is between point a and point b. Any unpolymerized emulsion was removed by pressured nitrogen. After an extra 15 s of illumination time for complete curing, the chip with the monolithic structure was flushed with Milli-Q water at a flow rate of $15 \text{ } \mu\text{l/min}$. All the inlets and outlets of the chip were sealed for storage purposes.

Enzyme immobilization

Pepsin was immobilized onto the monolithic support based on the protocol published by Jönsson et al. [51]. A total of 200 μl of 2-(boc amino)ethanethiol containing 0.5% v/v photoinitiator (Lucirin TPO-L) was pumped into the monolithic channel and exposed under collimated UV light for 30 s, aiming at introducing amine groups at the surface of the monolith. Afterwards, the monolith was rinsed with Milli-Q water at $10 \text{ } \mu\text{l/min}$ for 5 min to remove unreacted products. The exposure (de-protection) of amine groups at the surface of the monolith was carried out by flushing with hydrochloric acid overnight (4 M, 12 h), at a flow rate of $2 \text{ } \mu\text{l/min}$. After washing with Milli-Q water at $30 \text{ } \mu\text{l/min}$, the channel was filled with ascorbic acid solution (100 mg in 1.5 ml 66% methanol) and incubated for 30 min, followed by rinsing with Milli-Q water (5 min, $30 \text{ } \mu\text{l/min}$). Ascorbic acid establishes a covalent linkage between the amine groups on the surface of the monolith and primary amino groups of the enzyme.

Subsequently, pepsin was immobilized on the activated monolithic material by introducing 10 mg/ml pepsin solution in Milli-Q water and incubated while sealed for 24 h at 4 °C. Non-absorbed enzyme was removed by pumping Milli-Q water through the reactor before use. After immobilization, outlet A in ESM Fig. S1d was sealed completely through photopolymerization using 0.2% (v/v) Lucirin TPO-L in thiol-ene. The enzymatic microreactor was filled with 0.1 M sodium acetate in 10% glycerol at 10 µl/min for storage.

Digestion off-chip

A total of 300 µl of pepsin-immobilized beads was mixed with 900 µl 0.23% FA in Milli-Q water to get a homogeneous suspension. Pepsin beads were separated by centrifugation at 500 rpm for 2 min and the supernatant was discarded. This washing procedure was repeated twice. 1.0 mg of Glu-fib was dissolved in 200 µl of 0.23% FA in Milli-Q water and added to the tube containing final pepsin beads. The mixture of suspension was incubated for 15 min at 37 °C in a shaker. The suspension was transferred to a separator tube and centrifuged at 2000 rpm for 2 min to stop the reaction and obtain particle-free digestion product solution.

Fabrication of 3D-printed mask and holders

A 3D-printed lithographic mask (pocket dimensions, 77 × 27 × 1 mm) was used to selectively place monolith in a channel right before photopolymerization, with a slit of 12 ± 1.5 mm for exposure (ESM Fig. S1). Fluidic connection to the microfluidic device was realized through 3D-printed holders with tubes assembled. The chip holders and mask models were designed with computer-aided design software (Autodesk Fusion 360, San Rafael, CA, USA) and exported to an “Ultimaker 2” 3D printer (Ultimaker, Geldermalsen, The Netherlands). Black polylactic acid-loaded filaments (PLA, Innofil3D, Emmen, The Netherlands) were utilized for the 3D printer, with the main parameter settings as 1.05 mm wall thickness, 0.1 mm layer height, and 100% infill.

Experimental setup and data collection

Fluidic sealing was realized by assembling 6–32 coned MicroTight® fittings (IDEX Health & Science LLC, Oak Harbor, WA, USA), PEEK tubings (1/32" × 0.38 mm/.015" ID, JR-T-5715-M3, VICI Jour, Switzerland), and in-house fabricated cylindrical PDMS O-rings, which partly integrated into the two 3D-printed holders. Silicone tubes were fixed to the four end holes of the side electrode grooves using epoxy glue (ESM Fig. S1e).

Pulsation-free syringe pumps (Fusion 200, Chemyx, USA; LEGATO® 110, KD Scientific, USA) were used to introduce hydrodynamic flow into buffer inlets, electrode channels, and

central sample inlet (Fig. 1a). High-precision glass syringes (PTFE Luer lock, VWR, Søborg, Denmark) were connected to PEEK tubings. Prior to the experiments, the chip was flushed with ethanol and Milli-Q water, followed by 10-min priming with separation buffer. For this purpose, four-port switch valves were utilized between syringes and inlets of the chip to get rid of bubbles when changing priming solvents. After experiments, the chip was flushed thoroughly for 10 min with Milli-Q water and ethanol, respectively.

Platinum electrodes were inserted into the side silicone tubes and connected with a high voltage power supply (High Voltage Sequencer, Labsmith HVS448 6000D) (ESM Fig. S1e). The electrical potential was controlled through computer-aided software. The chip was observed and monitored under a Nikon Eclipse Ti fluorescence microscope (Eclipse Ti-E, Nikon Instruments Europe BV, The Netherlands) equipped with an Andor Neo camera (Belfast, Ireland) and Nikon NIS-elements AR software (Tokyo, Japan). The separations were observed with filter sets for FITC (excitation peak 495 nm, emission peak 519 nm, Nikon) and TRITC (excitation peak 558 nm, emission peak 575 nm, Nikon), respectively. For large images exceeding the camera field of view, multiple image frames across the area of the separation chamber were captured, combined, and stitched together with 10% overlay. Line scan acquisition was processed using ImageJ (Rasband, National Institutes of Health, USA), and the contrast of images was adjusted for better observation. For easy use of the fabricated chip with an inverted fluorescence microscope, and assembling the two 3D-printed holders together, the backplate was cut from PMMA substrate, using a desktop laser (Epilog Mini18 CO2 laser, Epilog laser, CO, USA).

The mass spectrometry measurements were carried out with an Agilent 1100-series HPLC coupled to Micromass Quattro Micro™ system, using an electrospray ionization source in positive mode. The mobile phases, consisting of 0.1% (v/v) formic acid in water (A) and 0.1% (v/v) formic acid in acetonitrile (B), were pumped at a flow rate of 0.2 ml/min. The injection volume was 5 µl. The capillary voltage was set at 3.50 kV, and the cone voltage was 30 V. The desolvation gas flow was set to 650 l/h at a temperature of 300 °C, and the source temperature was set to 80 °C. The cone gas flow was 20 l/h. The data was monitored in full-scan mode.

Results and discussion

Chip design

In this study, we used so-called partitioning bars to keep bubbles from entering the main chamber; this was based on a design published previously [52]. The resulting thiol-ene chips (Fig. 1) are 27 mm × 77 mm in size with

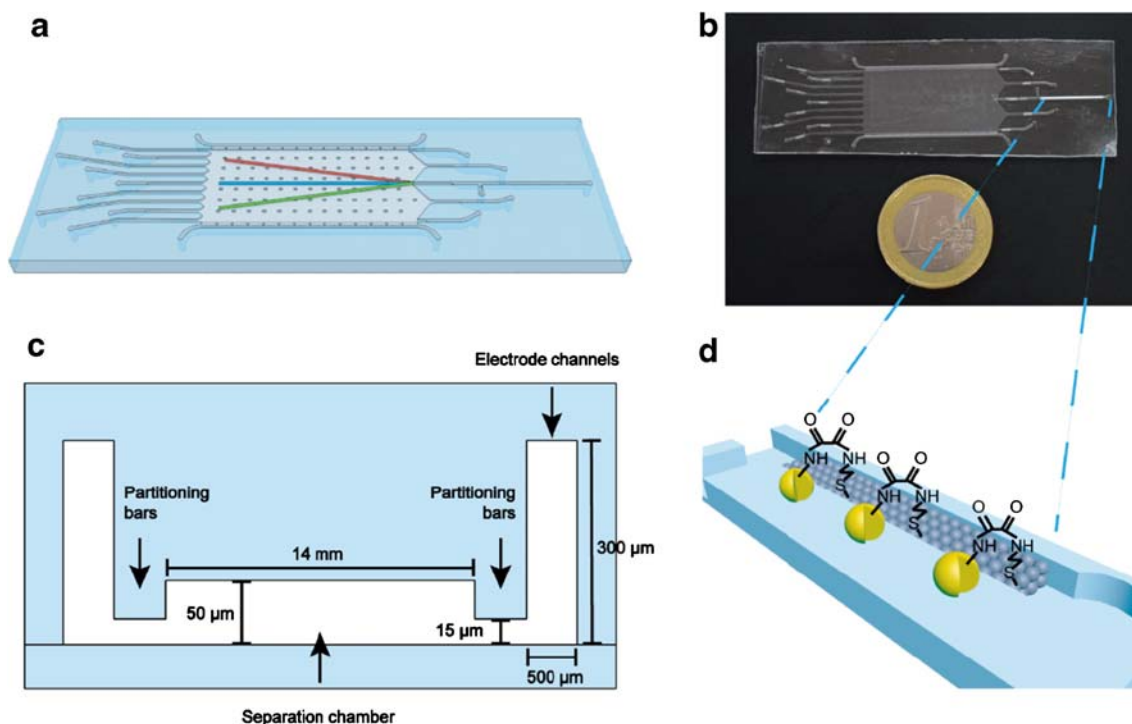


Fig. 1 Chip design. **a** 3D sketch of the entire chip. **b** Photograph of the IMER-FFE device, with immobilized enzyme. **c** Cross-sectional structure of the separation area chamber and electrode channels (not to scale). **d** Zoom-in from **(b)**: schematic depiction of IMER

a total thickness of 1 mm, consisting of five chamber inlets for sample solution and running buffer, nine outlets for downstream sample collection, and one inlet and outlet on each lateral side for the electrode channels. The microreactor was incorporated into the middle inlet channel, being 12 mm long \times 200 μ m deep \times 500 μ m wide, and with a slope to 50 μ m over 2 mm that connects to the separation chamber. Figure 1d illustrates the immobilization of the enzyme in the microreactor via thiol-ene click chemistry and ascorbic acid linkage. The main chamber is 50 μ m deep, 14 mm wide, and 28 mm long. Inlet and outlet channels are 500 μ m wide and all end holes/openings are 800 μ m in diameter. Figure 1c shows the cross-sectional structure of the main chamber. The partitioning bars are 500 μ m wide and leave a gap of about 15 μ m in height; the purpose is to separate the main chamber from the electrode slots, which are 500 μ m \times 300 μ m (width \times height). This design prevents bubbles, which may be generated in the electrode compartments, from entering into the separation region. Pillars are introduced throughout the big chamber and also along the partitioning strips to prevent the two thiol-ene slabs from collapsing during the bonding process. One typical challenging issue in FFE devices is how to keep any electrolysis products generated at the electrodes by the applied electric field away from the main separation chamber. Bubbles at the interface between the separation and electrode compartments can

disrupt fluid flow and also influence the efficiency of the separation, especially if too many bubbles aggregate. Several design strategies have been used to eliminate bubbles from entering the separation region. Membrane-like channels [53] and ion-permeable membranes [54] were microfabricated into the chip as barriers to isolate bubbles while permitting electrical contact, but their drawbacks were a high electrical resistance and the limited mechanical stability of the membranes. Electrostatic induction [55] of an electric field was demonstrated, and no electrolysis and current flow between the electrodes were observed. Fonslow et al. [56] used different channel depths between the electrode slots and the separation chambers to adjust flow velocities and remove bubbles by a 15 times higher flow rate in the electrode channels. Replacement of standard electrodes with palladium electrodes [57] and salt bridge connections [58] also contributed to suppressing bubble formation. Although these approaches were shown to alleviate the detrimental effect of bubbles, some of them have complicated microchip fabrication procedures due to the more laborious membrane or electrode incorporation, and thus often also increased the costs of the devices. In the current study, we used partitioning bars to isolate bubbles, which are manufactured easily and economically. External electrodes were used as a straightforward and effective alternative for providing electrical contact, inspired by Köhler et al. [52], thus also

simplifying the fabrication by avoiding integration of electrodes.

Characterization of FFE on a thiol-ene device

In a first experiment, the thiol-ene polymer-based device was applied to free-flow separation of a mixture of fluorescent dyes. The velocities and widths of sample streams were adjusted by changing the parameters of the syringe pumps. Figure 2a and c show the separation of 2',7'-dichlorofluorescein and rhodamine 6G (note: not the entire width of the separation chamber is shown). The separated bands appeared immediately once the electric field was applied to the device. Line scans were taken at a distance of 7 mm upstream from the exit of the main chamber. Under the experimental conditions used here (20 mM HEPES at pH 7.5), 2',7'-dichlorofluorescein has a negative charge of one, resulting in its deflection to the anode, while rhodamine 6G carries one positive charge so the stream migrates to the cathode. Figure 2b and d illustrate the separation of 2',7'-dichlorofluorescein and rhodamine B. Rhodamine B is not charged at these conditions and thus not influenced by the electrical field. The sample mixture split into two streams immediately once the electric field was applied. Sample streams with smooth trajectories can be seen in the separation chamber. The support pillars

within the chamber did only marginally influence the flow shape of the separated streams. It should be noted that the separation of the two streams is not proceeding in a strictly linear way, but has a slight “trumpet” shape, most likely due to the presence of discreet outlets towards the end of the separation chamber. An angulagram was constructed to evaluate the quality of the separation, following an approach published previously [59]. Briefly, the reflectometric digital image (aligned by mirroring and rotation from Fig. 2a) of the separation of DCF and R6G was transferred from Cartesian into polar coordinates, and the signal over radius was integrated. The reflectometric image (fluorescein.preview) can be found in the Python supplementary material (ESM Fig. P4). Parameters were imported into a Python program (ESM angureflexin.py) for developing an angulagram, and another Python program (ESM evolutin.py) for computing characteristics including stream deflection, width, linearity, and resolution. As shown in Fig. 3, the streams are narrow ($\omega < 3.0^\circ$) and linear ($L^2 \geq 0.90$). The original image, evaluation of data produced by Python, and the source code are provided in the ESM. The electric field strength and the flow rate are the main factors that influence the separation performance in an FFE device. Figure 4a–c show the effects of the electrical field strength as well as the buffer flow rate on the separation of 2',7'-

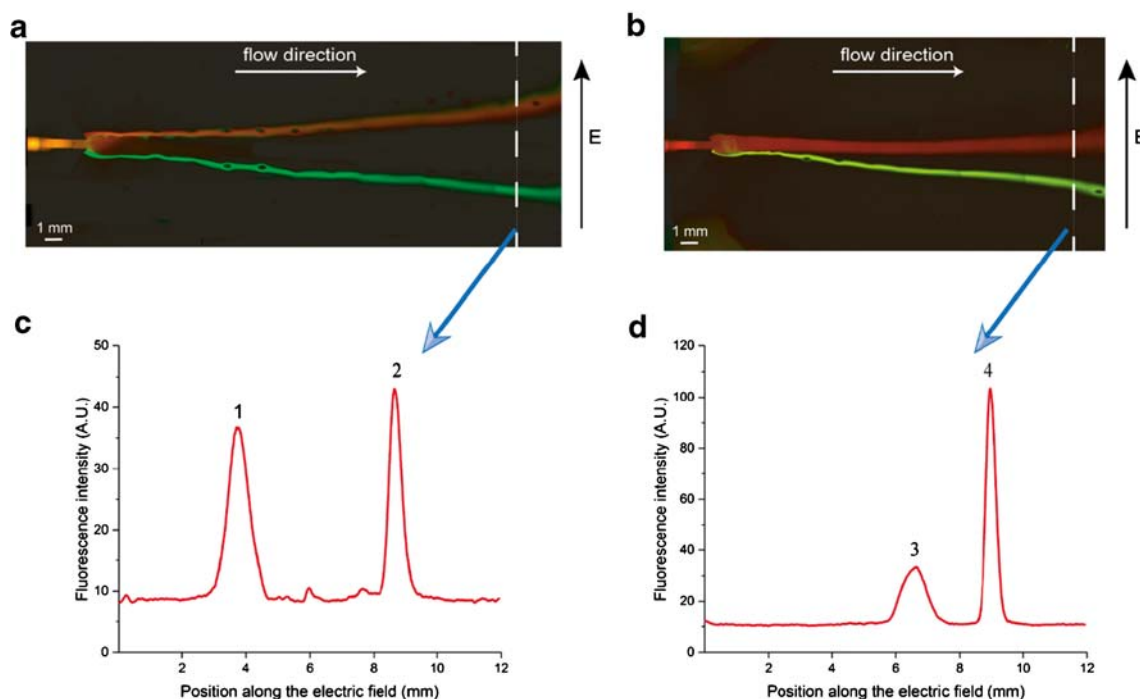


Fig. 2 FFE separation of fluorescent dyes. **a** FFE separation of 2',7'-dichlorofluorescein and rhodamine 6G. **b** FFE separation of 2',7'-dichlorofluorescein and rhodamine B. **c** Corresponding line scan from near the exit of the main chamber, as indicated by the white line in a;

(1) rhodamine 6G, (2) 2',7'-dichlorofluorescein. **d** corresponding line scan from near the exit of the main chamber, as the white line in b; (3) rhodamine B, (4) 2',7'-dichlorofluorescein. Separation in 20 mM HEPES buffer pH 7.5 at a field strength of 429 V/cm

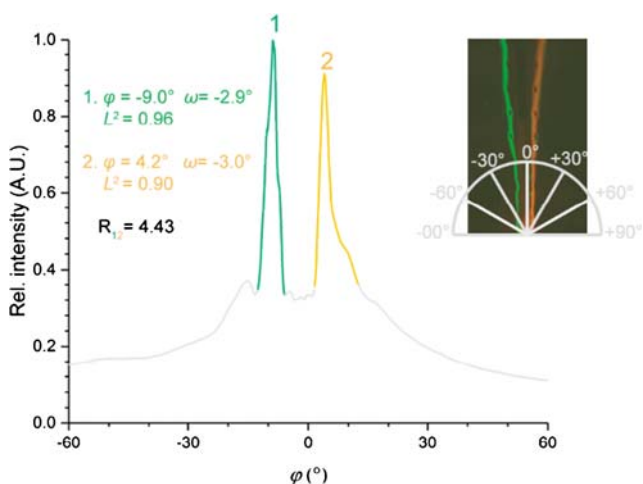


Fig. 3 Angulagram of the separation of DCF and R6G. The values in the graph are stream deflection (φ), width (ω), linearity (L^2), and resolution (R) between two streams

dichlorofluorescein and rhodamine 6G. All the cross sections were taken from the same position in the separation chamber as indicated by the white line in Fig. 2a. Separation efficiencies obtained under different conditions were compared. Generally speaking, visual inspection alone shows that the spatial separation between

the two bands increased with increasing field strength, but the peaks also got broader.

Resolution values were calculated to more quantitatively characterize the separation efficiency, using an equation suggested by Fonslow and Bowser [60]:

$$R = 2(d_1 - d_2) / (W_1 + W_2)$$

where d_1 and d_2 are the migration distances perpendicular to the centerline direction and W_1 and W_2 are the widths of the streams. Figure 4d demonstrates the relationship between resolution, applied electric field strength, and flow rate of the buffer solution. As expected, the resolution increases when higher field strengths are applied. At the same time, lower buffer flow rates yield better resolution of the sample inside the separation chamber.

In an FFE device, the migration distance, d , along the direction of the applied voltage can be described by the equation below [60]:

$$d = Et\mu_{\text{total}} = EL\mu_{\text{total}}/v$$

where E is the electric field strength, t is the residence time spent in the separation compartment, μ_{total} is the total mobility of analyte, L is the longitudinal distance a given analyte

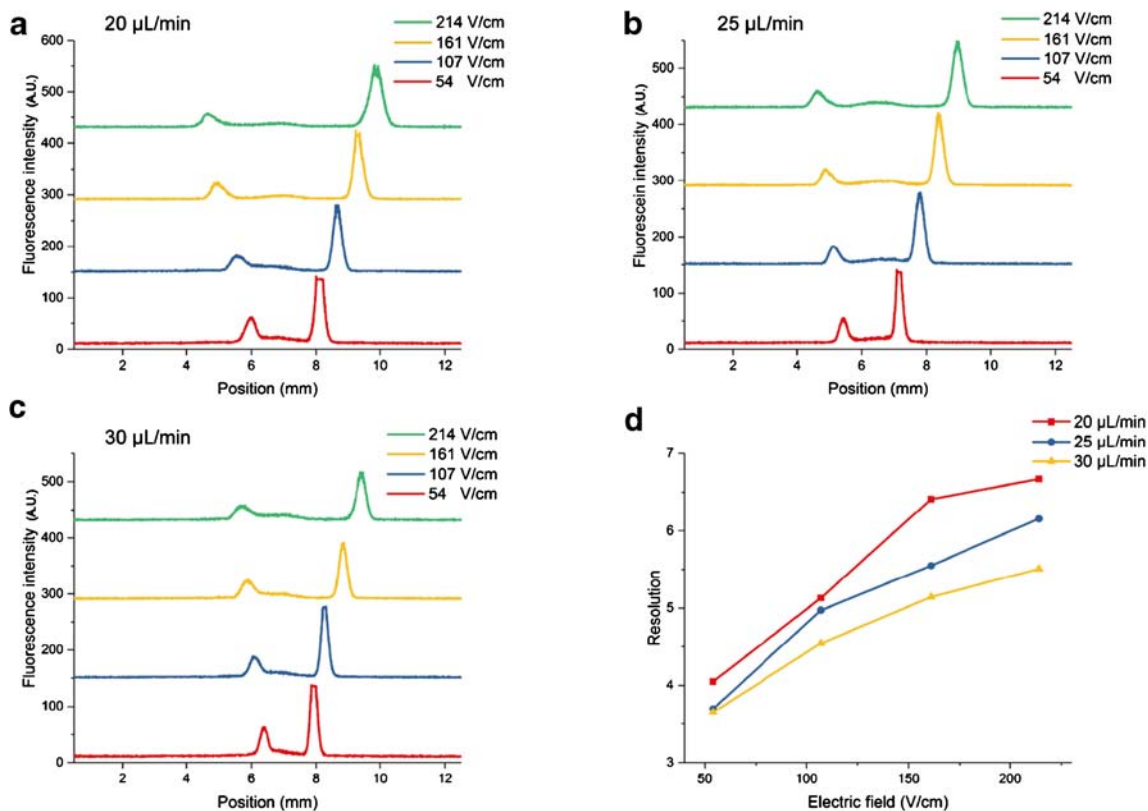


Fig. 4 FFE separation efficiency of 2',7'-dichlorofluorescein and rhodamine 6G at different electric field strengths and for different buffer flow rates. **a** 20 $\mu\text{L}/\text{min}$, **b** 25 $\mu\text{L}/\text{min}$, and **c** 30 $\mu\text{L}/\text{min}$. **d** Resolution

between the two fluorescent dyes calculated from (a), (b), and (c). Electropherograms are offset for clarity

migrates prior to the detection point, and v is the linear velocity of the carrier buffer. Electric field strength and residence time are thus two important and independent parameters that determine the migration distance. Et is defined as separation power [61], which is used to predict the migration distance by adjusting electric field and velocity

$$\text{separation power} = Et = EL/v$$

Experimentally, separation profiles under two different conditions (30 $\mu\text{l}/\text{min}$ flow rate at 161 V/cm field strength, and 20 $\mu\text{l}/\text{min}$ at 107 V/cm (two-thirds of the previous values)) were compared. Both DCF ($d = 1.7$ mm) and R6G ($d = 1.3$ mm) had the same migration distance under both conditions, yielding the same separation power, as expected. This means that the electric field strength and the linear velocity of the hydrodynamic flow provide means to adjust separation conditions and, here, keep the same position of the streams.

Contributions from the injection (σ_{inj}^2), from diffusion (σ_{D}^2), and from hydrodynamic broadening (σ_{HD}^2) are the major sources of band broadening [60].

$$\sigma_{\text{total}}^2 = \sigma_{\text{inj}}^2 + \sigma_{\text{D}}^2 + \sigma_{\text{HD}}^2 = \frac{\omega_{\text{inj}}^2}{12} + \frac{2DL}{v} + \frac{h^2 d^2 v}{105DL}$$

where ω_{inj} is the width of the injection plug, D is the diffusion coefficient of the analyte, v is the linear velocity of the carrier buffer, d is the migration distance of the analyte, and L and h are the length and depth of the separation channel, respectively. According to the equation above, the total variance is

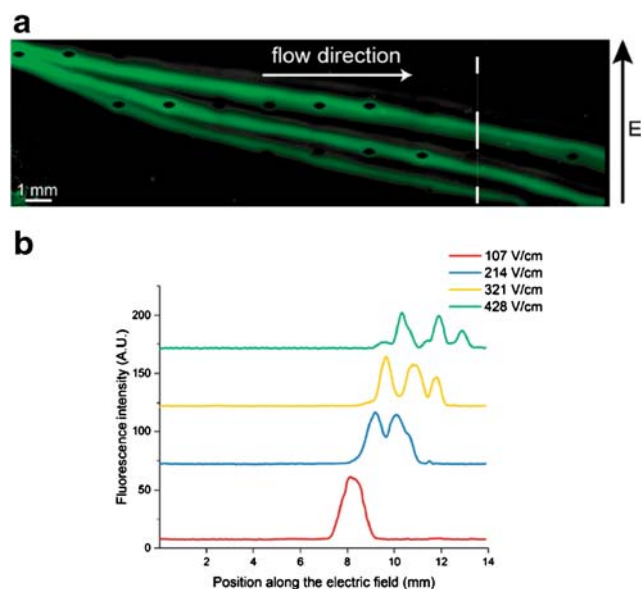


Fig. 5 Continuous separation of amino acids. **a** A fluorescent photograph of FITC-amino acids. Fluorescent bands from top to bottom: FITC-S-butylamine (upper stream), FITC-glycine (middle stream), and FITC-L-aspartic acid (lower stream). **b** Chip separation using different electric field strengths

proportional to the square of the deflection distance at a given flow rate and in the same device. This is in accordance with Fig. 4a, where the peak width increases when a band deflects more. In this case, hydrodynamic broadening is the major source of band broadening. Decreasing the height of the separation chamber could help to minimize the effect of hydrodynamic broadening, and Joule heating would decrease at the same time (another potential contribution to band broadening).

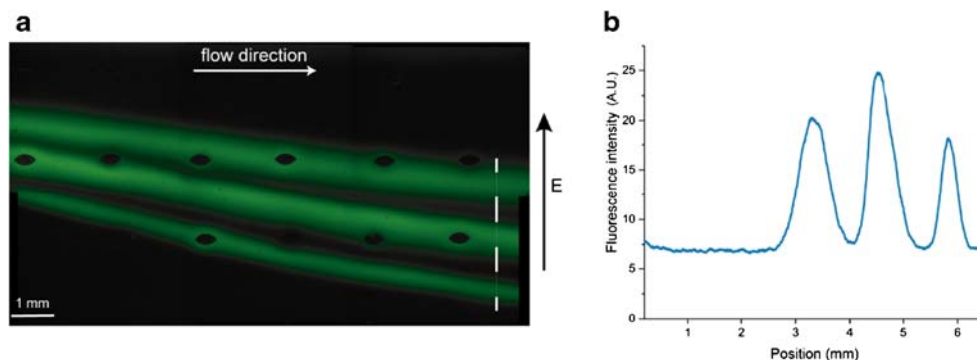
Separation of fluorescently labeled amino acids

After the initial performance evaluation with fluorescent dyes, we focused on the application of this device to amino acids. Aspartic acid, glycine, and butylamine were selected as target analytes and labeled with FITC for detection. Figure 5a presents an image of the μFFE separation of the mixture of fluorescently labeled amino acids using 5 mM borate buffer at pH 8. Line scans were taken at the dashed line and separation efficiencies under various field strengths were studied. By labeling with FITC, two additional negative charges are added to the original charge state of the molecules under the chosen experimental condition. The order of migration distance depends on their electrophoretic mobilities, which are related to the molecules' mass/charge ratios. All analytes, which have FITC groups covalently coupled to the primary amines of their structures, deflected towards the anode, and the most negatively charged species, FITC-aspartic acid, migrated furthest. Separation resolution increased with increasing field strengths. It shows that improved resolutions can be obtained by applying higher electric field strengths when compounds have the same fluorescein group, which is covalently coupled, in their structures and similar size, and thus smaller difference in electrophoretic mobilities.

Continuous separation of fluorescently labeled peptides

The anticipated application of the combined microfluidics units is to perform enzymatic digestion and online separation of peptide fragments in a continuous fashion. Glu-fibrinopeptide (Glu-fib) was chosen as a model analyte to validate this setup. This oligopeptide consists of 14 amino acids with the sequence EGVNDNEEGFFSAR. Initially, Glu-fib was digested off-chip by using pepsin immobilized on beads, then labeled with FITC before being introduced to the FFE device. HPMC was added to the running buffer for a dynamic coating of the channel walls to decrease non-specific surface adsorption of peptides. Figure 6 shows three separated streams of fluorescently labeled digested fragments using 20 mM CHES buffer at pH 8. Pepsin is most likely to cleave at the carboxyl side of phenylalanine, and thus, the digested products are assumed to be the fragments SAR, FSAR, F, and

Fig. 6 Continuous separation of fluorescently labeled peptides. **a** Image of fluorescently labeled peptides after off-chip digestion with pepsin immobilized on beads. **b** Line scan from the white line in (a) (without characterization by mass spectrometry)



EGVNDNEEGF, respectively. Under the experimental condition of pH 8, the labeling agent FITC has two negative charges. EGVNDNEEGF and F have one primary amine group in their structures after the hydrolysis reaction and thus react with one molecule of FITC, such that they carry seven and three negative charges, respectively. SAR and FSAR both have five negative charges after the derivatization (and only one amino acid difference in mass/size), and therefore, both fragments co-migrate. Still, it could be demonstrated that the thiol-ene-based FFE device could be successfully applied for separation of larger molecules.

In-line peptide digestion with hyphenated FFE

While fluorescently labeled analytes make for nice visualizations of continuous separations in FFE, many relevant analytes, including most peptides, are not natively fluorescent. Even more important, labeled functional groups may have an effect on the properties and structures of the analytes (here: peptides), and also influence the separation performance. Thus, we introduced non-labeled Glu-fib to the IMER-FFE setup and collected digested peptides from the outlet at the end of the microreactor and identified them with mass spectrometric analysis. For a first evaluation of the enzyme reactor

part alone, a single IMER device was used, as shown in ESM Fig. S1a. Caffeine was chosen as an internal standard and added to the Glu-fib solution, in order to evaluate the immobilized enzymatic efficiency on-chip, and since pepsin preferentially only cleaves at the carboxyl side of aromatic amino acids, caffeine is not digested or otherwise affected by the enzyme. Figure 7a presents the mass signals of the involved molecules before on-chip digestion (caffeine, MW 195.185; Glu-fib, MW 785.833, EGVNDNEEGFFSAR). Figure 7b shows the mass signals of the digestion products collected from the outlet of the microreactor (MW 333.314, Ser-Ala-Arg (SAR); MW 480.430, Phe-Ser-Ala-Arg (FSAR); MW 166.092, Phe (F); MWs 1109.666/555.335/577.317, Glu-Gly-Val-Asn-Asp-Asn-Glu-Glu-Gly-Phe (EGVNDNEEGF)), which were identified as sequences of amino acids. Here, we could only see less than 2% of Glu-fib remaining (by comparing the response ratio of Glu-fib to the internal standard after and before digestion), which means the peptide was largely digested in the microreactor. Subsequently, the entire IMER-FFE device was used to perform in-line digestion followed by continuous electrophoretic separation using 10 mM ammonium acetate buffer at pH 4.5. Figure 8a illustrates the stream of rhodamine 110, which carries almost no charge under the experimental condition. It

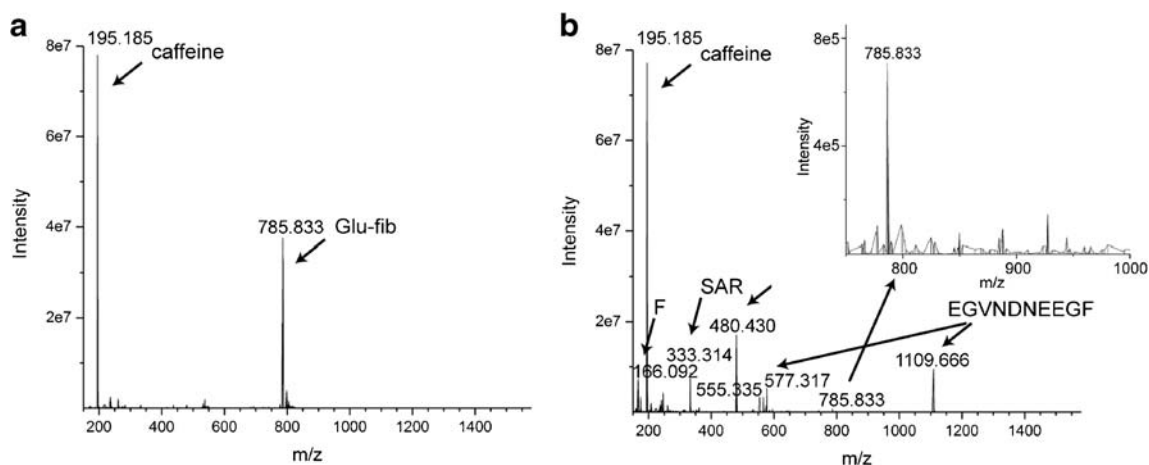


Fig. 7 MS of fragments from the IMER device. **a** Glu-fib before digestion and caffeine used as an internal standard. **b** Products collected from the outlet of the microreactor (fragments identified by the amino acid sequence)

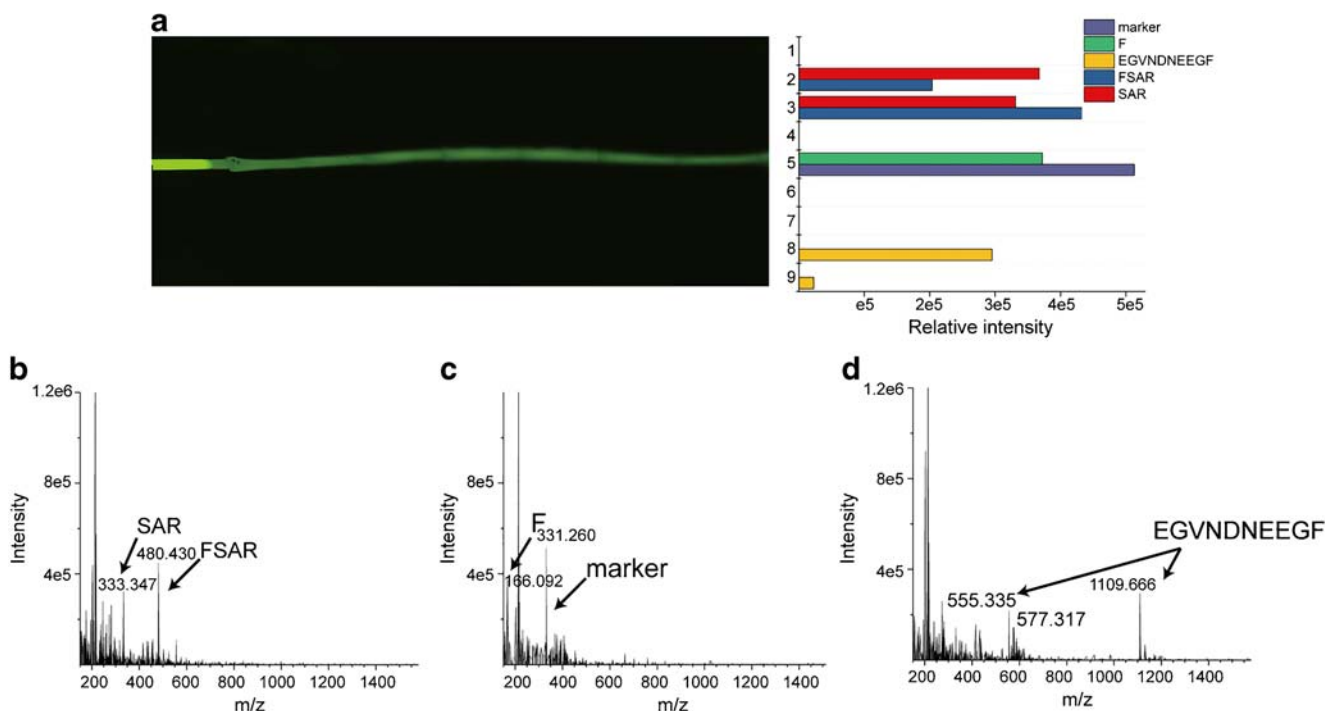


Fig. 8 a Photo with a fluorescent marker in the center and nine outlets labeled. MS spectrum of fragments from the IMER-FFE device. Samples collected from **b** outlet 3, **c** outlet 5, and **d** outlet 8

was chosen as a visual marker to be able to adjust the flow rates of the syringe pumps and obtain a straight line. The intensities of fragments collected from outlets 1–9 (see also Fig. 1a) are summarized next to the electrophoretic image. EGVNDNEEGF is negatively charged under the experimental conditions, and thus, outlets 5–9 are likely to contain this fragment. The positively charged SAR and FSAR ideally should exit from the upper outlets (1–4). Figures 8b–d show the samples collected from outlets 2/3 (MW 333.347, SAR; MW 480.430, FSAR), outlet 5 (MW 166.092, F; 331.260, marker), and outlets 8/9 (MW 1109.666/555.335/577.317, EGVNDNEEGF), which is in accordance with our expectation. SAR and FSAR were both detected from outlets 2 and 3, where SAR was collected from outlet 2 at a higher concentration while FSAR tends to be found more in outlet 3. Apparently, baseline separation was not achieved for these two species under the chosen conditions, which is mainly due to their similarity in molecular structure and the same charge state. However, the results suggest that we can separate peptide fragments from protein digestion and continuously collect them at different outlets using this IMER-FFE device.

Conclusion

In this study, we developed a robust and simple enzyme reactor hyphenated with a free-flow electrophoretic separation microfluidic platform. This is the first time thiol-ene polymers were used to manufacture all fluidic elements, the

monolith support for the enzyme reactor, and the FFE unit. After an initial characterization with fluorescent dyes and amino acids and an investigation on how different parameters influence separation efficiency, the two functional units were integrated and the digestion and separation were completed in a few seconds. The online coupling of this all-thiol-ene-based system demonstrates its potential for avoiding tedious and time-consuming sample transfer, decreasing incubation time compared with traditional enzymatic approach, minimizing sample volume consumption, and allowing repeated usage. It extends the application of FFE and could be considered a potential tool for online chip-based peptide analysis. The continuous separation approach also allows for collection of larger amounts of analytes, improving in particular mass-dependent detection. In the future, a direct coupling of this current IMER-FFE device to mass spectrometry [62–66] will further strengthen the potential for automation. Even though coupling the devices to MS detection does not require fluorescent labeling and may allow both better sensitivity and selectivity, it is not a trivial task and not as robust as optical detection. The spray stability is highly dependent on the geometry of the spray tip and how the electric contact for the electrospray voltage is applied at the spray tip. Overall, the whole fabrication of the device becomes much more complicated and the performance of the device is highly dependent on the spray performance. Currently, we are working on optimizing the ESI emitter and will integrate it with the described setup in the near future.

Funding information The present study is supported financially by the Chinese Scholarship Council (CSC). AK received support from the Independent Research Council of Denmark (DFF) under contract 7017-00267.

Compliance with ethical standards

Conflict of interest The authors declare that they have no conflicts of interest.

References

- Kirk O, Borchert TV, Fuglsang CC. Industrial enzyme applications. *Curr Opin Biotech.* 2002;13(4):345–51. [https://doi.org/10.1016/s0958-1669\(02\)00328-2](https://doi.org/10.1016/s0958-1669(02)00328-2).
- Hasan F, Shah AA, Hameed A. Industrial applications of microbial lipases. *Enzym Microb Technol.* 2006;39(2):235–51. <https://doi.org/10.1016/j.enzmictec.2005.10.016>.
- Manabe T, Jin Y, Tani O. Assignment of human plasma polypeptides on a nondenaturing 2-D gel using MALDI-MS and PMF and comparisons with the results of intact protein mapping. *Electrophoresis.* 2007;28(5):843–63. <https://doi.org/10.1002/elps.200600389>.
- Chang JP, Kiehl DE, Kennington A. Separation and characterization of the tryptic peptide mapping of recombinant bovine growth hormone by reversed-phase high-performance liquid chromatography electrospray mass spectrometry. *Rapid Commun Mass Spectrom.* 1997;11:1266–70.
- Zhang Y, Fonslow BR, Shan B, Baek M-C, Yates JR. Protein analysis by shotgun/bottom-up proteomics. *Chem Rev.* 2013;113(4):2343–94. <https://doi.org/10.1021/cr3003533>.
- Matosevic S, Szita N, Baganz F. Fundamentals and applications of immobilized microfluidic enzymatic reactors. *J Chem Technol Biotechnol.* 2011;86(3):325–34. <https://doi.org/10.1002/jctb.2564>.
- Miyazaki M, Maeda H. Microchannel enzyme reactors and their applications for processing. *Trends Biotechnol.* 2006;24(10):463–70. <https://doi.org/10.1016/j.tibtech.2006.08.002>.
- Shi J, Zhao W, Chen Y, Guo L, Yang L. A replaceable dual-enzyme capillary microreactor using magnetic beads and its application for simultaneous detection of acetaldehyde and pyruvate. *Electrophoresis.* 2012;33(14):2145–51. <https://doi.org/10.1002/elps.201200090>.
- Safdara M, Sproß J, Jänis J. Microscale immobilized enzyme reactors in proteomics: latest developments. *J Chromatogr A.* 2014;1324:1–10. <https://doi.org/10.1016/j.chroma.2013.11.045>.
- Girelli AM, Mattei E. Application of immobilized enzyme reactor in on-line high performance liquid chromatography: a review. *J Chromatogr B.* 2005;819(1):3–16. <https://doi.org/10.1016/j.jchromb.2005.01.031>.
- Peterson DS, Rohr T, Svec F, Fréchet MJ. Enzymatic microreactor-on-a-chip: protein mapping using trypsin immobilized on porous polymer monoliths molded in channels of microfluidic devices. *Anal Chem.* 2002;74(16):4081–8. <https://doi.org/10.1021/ac020180q>.
- Hajba L, Guttman A. Continuous-flow biochemical reactors: biocatalysis, bioconversion, and bioanalytical applications utilizing immobilized microfluidic enzyme reactors. *J Flow Chem.* 2016;6(1):8–12. <https://doi.org/10.1556/1846.2015.00028>.
- Keckskemeti A, Gaspar A. Particle-based immobilized enzymatic reactors in microfluidic chips. *Talanta.* 2018;180:211–28. <https://doi.org/10.1016/j.talanta.2017.12.043>.
- Wang C, Oleschuk R, Ouchen F, Li J, Thibault P, Harrison DJ. Integration of immobilized trypsin bead beds for protein digestion within a microfluidic chip incorporating capillary electrophoresis separations and an electrospray mass spectrometry interface. *Rapid Commun Mass Spectrom.* 2000;14:1377–83.
- Terry SC, Jerman JH, Angell JB. A gas chromatographic air analyzer fabricated on a silicon wafer. *IEEE Trans Electron Devices.* 1979;26:1880–6.
- Jang L-S, Liu H-J. Fabrication of protein chips based on 3-aminopropyltriethoxysilane as a monolayer. *Biomed Microdevices.* 2009;11(2):331–8. <https://doi.org/10.1007/s10544-008-9239-7>.
- Sticker D, Geczy R, Hafeli UO, Kutter JP. Thiol-ene based polymers as versatile materials for microfluidic devices for life sciences applications. *ACS Appl Mater Interfaces.* 2020. <https://doi.org/10.1021/acsaami.9b22050>.
- Hoyle CE, Lee TY, Roper T. Thiol-enes: chemistry of the past with promise for the future. *J Polym Sci A.* 2004;42(21):5301–38. <https://doi.org/10.1002/pola.20366>.
- Cramer NB, Bowman CN. Kinetics of thiol-ene and thiol-acrylate photopolymerizations with real-time Fourier transform infrared. *J Polym Sci A.* 2001;39(19):3311–9. <https://doi.org/10.1002/pola.1314>.
- Hoyle CE, Bowman CN. Thiol-ene click chemistry. *Angew Chem Int Ed.* 2010;49(9):1540–73. <https://doi.org/10.1002/anie.200903924>.
- Ashley JF, Cramer NB, Davis RH, Bowman CN. Soft-lithography fabrication of microfluidic features using thiol-ene formulations. *Lab Chip.* 2011;11(16):2772–8. <https://doi.org/10.1039/c1lc20189a>.
- Carlborg CF, Haraldsson T, Öberg K, Malkoch M, Wijngaart W. Beyond PDMS: off-stoichiometry thiol-ene (OSTE) based soft lithography for rapid prototyping of microfluidic devices. *Lab Chip.* 2011;11(18):3136–47. <https://doi.org/10.1039/c1lc20388f>.
- Sikanen TM, Lafleur JP, Moilanen M-E, Zhuang G, Jensen TG, Kutter JP. Fabrication and bonding of thiol-ene-based microfluidic devices. *J Micromech Microeng.* 2013;23(3):037002. <https://doi.org/10.1088/0960-1317/23/3/037002>.
- Khire VS, Yi Y, Clark NA, Bowman CN. Formation and surface modification of nanopatterned thiol-ene substrates using step and flash imprint lithography. *Adv Mater.* 2008;20(17):3308–13. <https://doi.org/10.1002/adma.200800672>.
- Zhang H, Cooper AI. Synthesis and applications of emulsion-templated porous materials. *Soft Matter.* 2005;1(2):107–13. <https://doi.org/10.1039/b502551f>.
- Lafleur JP, Senkbeil S, Novotny J, Nys G, Bøgelund N, Rand KD, et al. Rapid and simple preparation of thiol-ene emulsion-templated monoliths and their application as enzymatic microreactors. *Lab Chip.* 2015;15(10):2149–342. <https://doi.org/10.1039/c5lc00224a>.
- Wu Z, Zhang H, Li Q, Yang F, Li D. Capillary electrophoresis-based online immobilized enzyme reactor for beta-glucosidase kinetics assays and inhibitors screening. *J Chromatogr B.* 2019;1110-1111:67–73. <https://doi.org/10.1016/j.jchromb.2019.02.002>.
- Lin W, Skinner CD. Design and optimization of porous polymer enzymatic digestors for proteomics. *J Sep Sci.* 2009;32(15–16):2642–52. <https://doi.org/10.1002/jssc.200900221>.
- Křenková J, Klepárník K, Foret F. Capillary electrophoresis mass spectrometry coupling with immobilized enzyme electrospray capillaries. *J Chromatogr A.* 2007;1159(1–2):110–8. <https://doi.org/10.1016/j.chroma.2007.02.095>.
- Iqbal J. An enzyme immobilized microassay in capillary electrophoresis for characterization and inhibition studies of alkaline phosphatases. *Anal Biochem.* 2011;414(2):226–31. <https://doi.org/10.1016/j.ab.2011.03.021>.
- Min W, Wang W, Chen J, Wang A, Hu Z. On-line immobilized acetylcholinesterase microreactor for screening of inhibitors from natural extracts by capillary electrophoresis. *Anal Bioanal Chem.* 2012;404:2397–405. <https://doi.org/10.1007/s00216-012-6333-8>.

32. Wojcik R, Vannatta M, Dovichi NJ. Automated enzyme-based diagonal capillary electrophoresis: application to phosphopeptide characterization. *Anal Chem.* 2010;82:1564–7.
33. Li Y, Wojcik R, Dovichi NJ. A replaceable microreactor for on-line protein digestion in a two-dimensional capillary electrophoresis system with tandem mass spectrometry detection. *J Chromatogr A.* 2011;1218(15):2007–11. <https://doi.org/10.1016/j.chroma.2010.10.013>.
34. Liu L, Zhang B, Zhang Q, Shi Y, Guo L, Yang L. Capillary electrophoresis-based immobilized enzyme reactor using particle-packing technique. *J Chromatogr A.* 2014;1352:80–6. <https://doi.org/10.1016/j.chroma.2014.05.058>.
35. Mou S, Sun L, Wojcik R, Dovichi NJ. Coupling immobilized alkaline phosphatase-based automated diagonal capillary electrophoresis to tandem mass spectrometry for phosphopeptide analysis. *Talanta.* 2013;116:985–90. <https://doi.org/10.1016/j.talanta.2013.08.001>.
36. Schoenherr RM, Ye M, Vannatta M, Dovichi NJ. CE-microreactor-CE-MS/MS for protein analysis. *Anal Chem.* 2007;79:2230–8.
37. Wang T, Ma J, Zhu G, Shan Y, Liang Z, Zhang L, et al. Integration of capillary isoelectric focusing with monolithic immobilized pH gradient, immobilized trypsin microreactor and capillary zone electrophoresis for on-line protein analysis. *J Sep Sci.* 2010;33(20):3194–200. <https://doi.org/10.1002/jssc.201000324>.
38. Ye M, Hu S, Schoenherr RM, Dovichi NJ. On-line protein digestion and peptide mapping by capillary electrophoresis with post-column labeling for laser-induced fluorescence detection. *Electrophoresis.* 2004;25(9):1319–26. <https://doi.org/10.1002/elps.200305841>.
39. Peterson DS, Rohr T, Svec F, Fréchet JMJ. Dual-function microanalytical device by in situ photolithographic grafting of porous polymer monolith: integrating solid-phase extraction and enzymatic digestion for peptide mass mapping. *Anal Chem.* 2003;75:5328–35.
40. Cheng M, Wang R, Zhang B, Mao Z, Chen Z. Rapid proteolytic digestion and peptide separation using monolithic enzyme microreactor coupled with capillary electrophoresis. *J Pharm Biomed Anal.* 2019;165:129–34. <https://doi.org/10.1016/j.jpba.2018.11.063>.
41. Sakai-Kato K, Kato M, Toyo'oka T. Creation of an on-chip enzyme reactor by encapsulating trypsin in sol-gel on a plastic microchip. *Anal Chem.* 2003;75:388–93.
42. Turgeon RT, Bowser MT. Micro free-flow electrophoresis: theory and applications. *Anal Bioanal Chem.* 2009;394(1):187–98. <https://doi.org/10.1007/s00216-009-2656-5>.
43. Hannig K. Continuous free flow electrophoresis as an analytical and preparative method in biology. *J Chromatogr.* 1978;159:183–91.
44. Islinger M, Eckerskorn C, Völkl A. Free-flow electrophoresis in the proteomic era: a technique in flux. *Electrophoresis.* 2010;31(11):1754–63. <https://doi.org/10.1002/elps.200900771>.
45. Saar KL, Müller T, Charmet J, Challa PK, Knowles TPJ. Enhancing the resolution of micro free flow electrophoresis through spatially controlled sample injection. *Anal Chem.* 2018;90(15):8998–9005. <https://doi.org/10.1021/acs.analchem.8b01205>.
46. Arora A, Simone G, Salieb-Beugelaar GB, Kim JT, Manz A. Latest developments in micro total analysis systems. *Anal Chem.* 2010;82:4830–47.
47. Johnson AC, Bowser MT. Micro free flow electrophoresis. *Lab Chip.* 2017;18(1):27–40. <https://doi.org/10.1039/c7lc01105a>.
48. Whitesides GM. The origins and the future of microfluidics. *Nature.* 2006;442(7101):368–73. <https://doi.org/10.1038/nature05058>.
49. deMello AJ. Control and detection of chemical reactions in microfluidic systems. *Nature.* 2006;442(7101):394–402. <https://doi.org/10.1038/nature05062>.
50. Belder D. Towards an integrated chemical circuit. *Angew Chem Int Ed Engl.* 2009;48(21):3736–7. <https://doi.org/10.1002/anie.200900184>.
51. Jönsson A, Svejidal RR, Bøgelund N, Nguyen TTTN, Flindt H, Kutter JP, et al. Thiol-ene monolithic pepsin microreactor with a 3D-printed interface for efficient UPLC-MS peptide mapping analyses. *Anal Chem.* 2017;89(8):4573–80. <https://doi.org/10.1021/acs.analchem.6b05103>.
52. Köhler S, Benz C, Becker H, Beckert E, Beushausen V, Belder D. Micro free-flow electrophoresis with injection molded chips. *RSC Adv.* 2012;2(2):520–5. <https://doi.org/10.1039/c1ra00874a>.
53. Zhang C-X, Manz A. High-speed free-flow electrophoresis on chip. *Anal Chem.* 2003;75:5759–66.
54. Kohlheyer D, Besselink GAJ, Schlautmann S, Schasfoort RBM. Free-flow zone electrophoresis and isoelectric focusing using a microfabricated glass device with ion permeable membranes. *Lab Chip.* 2006;6(3):374–80. <https://doi.org/10.1039/b514731j>.
55. Janasek D, Schilling M, Manz A, Franzke J. Electrostatic induction of the electric field into free-flow electrophoresis devices. *Lab Chip.* 2006;6(6):710–3. <https://doi.org/10.1039/b602815b>.
56. Fonslow BR, Barocas VH, Bowser MT. Using channel depth to isolate and control flow in a micro free-flow electrophoresis device. *Anal Chem.* 2006;78:5369–74.
57. Macounová K, Cabrera CR, Yager P. Concentration and separation of proteins in microfluidic channels on the basis of transverse IEF. *Anal Chem.* 2001;73:1627–33.
58. Song Y-A, Chan M, Celio C, Tannenbaum SR, Wishnok JS, Han J. Free-flow zone electrophoresis of peptides and proteins in PDMS microchip for narrow pI range sample prefractionation coupled with mass spectrometry. *Anal Chem.* 2010;82:2317–25.
59. Ivanov NA, Liu Y, Kochmann S, Krylov SN. Non-aqueous continuous-flow electrophoresis (NACFE): separation complement for continuous-flow organic synthesis. *Lab Chip.* 2019;19:2156–60. <https://doi.org/10.26434/chemrxiv.7840937.v1>.
60. Fonslow BR, Bowser MT. Optimizing band width and resolution in micro-free flow electrophoresis. *Anal Chem.* 2006;78:8236–44.
61. Clifton MJ, Jouve N, Hd B, Sanchez V. Conditions for purification of proteins by free-flow zone electrophoresis. *Electrophoresis.* 1990;11:913–9.
62. Jönsson A, Lafleur JP, Sticker D, Kutter JP. An all thiol-ene microchip for solid phase extraction featuring an in situ polymerized monolith and integrated 3D replica-molded emitter for direct electrospray mass spectrometry. *Anal Methods.* 2018;10(24):2854–62. <https://doi.org/10.1039/c8ay00646f>.
63. Jender M, Novo P, Maehler D, Münchberg U, Janasek D, Freier E. Multiplexed online-monitoring of microfluidic free-flow electrophoresis via mass spectrometry. 2020.
64. Chartogne A, Tjaden UR, Greef JV. A free-flow electrophoresis chip device for interfacing capillary isoelectric focusing on-line with electrospray mass spectrometry. *Rapid Commun Mass Spectrom.* 2000;14:1269–74.
65. Benz C, Boomhoff M, Appun J, Schneider C, Belder D. Chip-based free-flow electrophoresis with integrated nanospray mass-spectrometry. *Angew Chem Int Ed Engl.* 2015;54(9):2766–70. <https://doi.org/10.1002/anie.201409663>.
66. Park JK, Campos CDM, Neužil P, Abelmann L, Guijt RM, Manz A. Direct coupling of a free-flow isotachopheresis (FFITP) device with electrospray ionization mass spectrometry (ESI-MS). *Lab Chip.* 2015;15(17):3495–502. <https://doi.org/10.1039/c5lc00523j>.

Publisher's note Springer Nature remains neutral with regard to jurisdictional claims in published maps and institutional affiliations.



Nan Lu is a PhD candidate from the Analytical Biosciences in the Department of Pharmacy at the University of Copenhagen, under the supervision of Professor Jörg P. Kutter. Her research focuses on the development of microfluidic devices for separation and detection techniques in the field of pharmaceutical analysis.



Nickolaj J. Petersen has a Master of Science in pharmacy and received his PhD degree in chemical engineering in 2002 from the Department of Micro and Nanotechnology at the Technical University of Denmark. He is Associate Professor at the University of Copenhagen, where his research mainly focuses on electrokinetic transport to develop new and improved ways of integrating miniaturized techniques for sample preparation and separations and their coupling to mass spectrometry.



Drago Sticker received his PhD degree in biomedical engineering from Vienna University of Technology (Austria) in 2015, where he worked with biosensing, organ-on-a-chip, and nano/microfabrication technologies. Following his PhD, he worked as Postdoctoral Researcher and Assistant Professor at the University of Copenhagen (Department of Pharmacy, Denmark), developing microfluidic solutions for protein analysis workflows. In 2019, he

joined Novo Nordisk A/S (Global Research Technologies, Denmark), where he works with oral drug delivery devices.



Jörg P. Kutter has more than 20 years of research and teaching experience with microchip-based analytical tools. Since September 2013, he has been Chair of Analytical Biosciences at the Department of Pharmacy at the University of Copenhagen. His research interests focus on the development of microfluidic devices for applications in the life sciences, and in particular the pharmaceutical sciences. He has published over 100 scientific articles.



Andreas Kretschmann studied chemistry at the Friedrich-Alexander University in Erlangen-Nürnberg, Germany. He received his PhD in environmental toxicology/chemistry at the Aquatic Research Institute Eawag/ETH in Dübendorf, Switzerland. Since 2018, he has been Associate Professor at the Department of Pharmacy, University of Copenhagen. His research focuses on the development of novel in vitro assays for the testing of drug enantiomers towards their endocrine disrupting potential.

assays for the testing of drug enantiomers towards their endocrine disrupting potential.